Babinet's principle for elastic waves: A numerical test

José M. Carcione[a)]
Osservatorio Geofisico Sperimentale, P.O. Box 2011 Opicina, 34016 Trieste, Italy

Anthony F. Gangi[b)]
Department of Geology and Geophysics, Texas A&M University, College Station, Texas 77843-3114

(Received 14 July 1997; accepted for publication 9 November 1998)

Babinet's principle states that the diffracted fields from complementary screens are the negative of each other. In electromagnetics, Babinet's principle for infinitely thin perfectly conducting complementary screens implies that the sum, beyond the screen plane, of the electric and the magnetic fields (adjusting physical dimensions) equals the incident (unscreened) electric field. A test of the principle for the elastodynamic case was made using numerical calculations, and the results demonstrate that Babinet's principle holds quite well for complementary plane screens with contrasting boundary conditions; that is, the complementary screen of a stress-free screen is a rigid screen with openings where the original stress-free screen existed, and vice versa. The results are exact in an anisotropic SH case; for the P–SV case, the diffracted waves, PdP, SdS, PdS, and SdP satisfy the principle exactly, while the refracted waves, PdPrSc and SdPrSc, do not satisfy the principle at all (these waves are generally much smaller than the PdS and SdP waves). Diffracted surface waves also do not satisfy the principle. The numerical method is based on a domain-decomposition technique that assigns a different mesh to each side of the screen plane. The effects of the screens on wave propagation are modeled through the boundary conditions, requiring a special boundary treatment based on characteristic variables. The algorithm solves the velocity/stress wave equations and is based on a Fourier/Chebyshev differential operator. © *1999 Acoustical Society of America.* [S0001-4966(99)01403-4]

PACS numbers: 43.20.Bi, 43.20.Gp, 43.20.Px [DEC]

INTRODUCTION

Babinet's principle was originally used to relate the diffracted-light fields by complementary thin screens.[1] A complementary screen is a plane screen with opaque areas where the original plane screen had transparent areas. Roughly speaking, the principle states that behind the diffracting plane, the sum of the fields associated with a screen and with its complementary screen is just the field that would exist in the absence of any screen; that is, the diffracted fields from the two complementary screens are the negative of each other and cancel when summed. The principle was later extended to electromagnetic fields and perfectly conducting plane screens or diffractors.[2,3]

Gangi and Mohanty[4] investigated Babinet's principle for elastodynamic fields and nonplanar complementary screens by using the representation theorem (see, for example, Gangi[5]). They performed elastic-wave experiments using thin polystyrene sheets where wave propagation is practically two-dimensional. The experiments considered rigid complementary screens, stress-free complementary screens, and mixed rigid/stress-free complementary screens. The results did not provide conclusive evidence about the conditions for which the principle is valid, mainly due to the experimental errors and the fact that the ''rigid'' screen was not perfectly rigid.

To the best of our knowledge, no attempt has been made to test Babinet's principle by numerical-modeling techniques. The present work considers rigid and stress-free (weak) boundary conditions on the screens in order to reproduce the laboratory experiments performed by Gangi and Mohanty.[4] The numerical algorithm is based on a domain-decomposition technique,[6–8] where the implementation of the boundary conditions requires a special treatment based on characteristic variables. Then, the governing equations are solved by a grid method that uses the Chebyshev differential operator in the direction normal to the screen plane, and the Fourier differential operator parallel to the screen plane.

The principle is investigated in the isotropic case, as in Gangi and Mohanty,[4] and for SH propagation through the symmetry plane of a monoclinic medium and qP–qS propagation in a transversely isotropic solid whose symmetry axis is perpendicular to the screen plane. These numerical simulations provide an adequate test of the principle, in view of the different constitutive equations and wave-propagation modes.

Babinet's principle would be of value since it allows us to obtain the solution of the complementary problem from the solution of the original problem without any additional effort. Moreover, it provides a check of the solutions for problems that are self-complementary (e.g., the problem of a plane wave normally incident on a half plane). Finally, it adds to our knowledge of the complex phenomena of elastic-wave diffraction.

[a)]Electronic mail: carcione@gems755.ogs.trieste.it
[b)]Electronic mail: gangi@tamu.edu

I. 2-D ELASTODYNAMIC EQUATION OF MOTION

The elastodynamic solution makes use of the equations of momentum conservation and the stress/particle–velocity relations, that can be written as

$$\frac{\partial \mathbf{v}}{\partial t}=\mathbf{A}\frac{\partial \mathbf{v}}{\partial x}+\mathbf{B}\frac{\partial \mathbf{v}}{\partial z}+\mathbf{f}, \tag{1}$$

where the parameters **A**, **B**, **v**, and **f** are explicitly given in the following subsections for the 2-D anisotropic case.

A. SH equation of motion

The particle–velocity/stress vector of the pure shear wave propagating in a monoclinic medium of arbitrary orientation (i.e., the normal to the isotropy plane makes an angle θ with the vertical z axis) is

$$\mathbf{v}=[v,\sigma_{xy},\sigma_{zy}]^{\mathsf{T}}; \tag{2}$$

$$\mathbf{A}=\begin{bmatrix}0 & \rho^{-1} & 0\\ C_{66} & 0 & 0\\ C_{46} & 0 & 0\end{bmatrix},\quad \mathbf{B}=\begin{bmatrix}0 & 0 & \rho^{-1}\\ C_{46} & 0 & 0\\ C_{44} & 0 & 0\end{bmatrix}, \tag{3}$$

where ρ is the material density and C_{IJ} are elastic constants

$$C_{44}=c_{44}\cos^4\theta+c_{66}\sin^4\theta, \tag{4}$$

$$C_{66}=c_{44}\sin^4\theta+c_{66}\cos^4\theta, \tag{5}$$

$$C_{46}=(c_{44}+c_{66})\cos^2\theta\sin^2\theta, \tag{6}$$

and the c_{IJ} are the elastic moduli in the principal axes system; i.e., when the z [or (3)] axis is the normal to the isotropy plane. Moreover,

$$\mathbf{f}=[f,0,0]^{\mathsf{T}} \tag{7}$$

is the body-force vector.

We recall that propagation in the plane of mirror symmetry of a monoclinic medium is the most general situation for which antiplane strain motion exists in all directions (the corresponding waves are also termed type-II S in the geophysical literature[9]). A detailed analysis of wave propagation of antiplane waves can be found in Carcione,[10] who studied the propagation of homogeneous plane waves in a viscoelastic medium.

B. qP–qS equation of motion

In a transversely isotropic medium, there are three wave solutions, two coupled modes denoted by qP and qS, representing the quasicompressional and quasishear modes, and the pure shear (SH) mode.[11] Since the medium has azimuthal symmetry, it is enough to consider qP–qS propagation in, say the (x,z) plane. The particle–velocity/stress vector and corresponding matrices are

$$\mathbf{v}=[v_x,v_z,\sigma_{xx},\sigma_{zz},\sigma_{xz}]^{\mathsf{T}}, \tag{8}$$

$$\mathbf{A}=\begin{bmatrix}0 & 0 & \rho^{-1} & 0 & 0\\ 0 & 0 & 0 & 0 & \rho^{-1}\\ c_{11} & 0 & 0 & 0 & 0\\ c_{13} & 0 & 0 & 0 & 0\\ 0 & c_{55} & 0 & 0 & 0\end{bmatrix}, \tag{9}$$

$$\mathbf{B}=\begin{bmatrix}0 & 0 & 0 & 0 & \rho^{-1}\\ 0 & 0 & 0 & \rho^{-1} & 0\\ 0 & c_{13} & 0 & 0 & 0\\ 0 & c_{33} & 0 & 0 & 0\\ c_{55} & 0 & 0 & 0 & 0\end{bmatrix}, \tag{10}$$

where c_{IJ} are the elastic moduli in the principal axes system and

$$\mathbf{f}=[f_x,f_z,0,0,0]^{\mathsf{T}}. \tag{11}$$

II. BABINET'S PRINCIPLE FOR ELASTIC WAVES

Consider a screen S, and its complementary screen C, and assume that the total field in the presence of S is $\mathbf{v}_S$ and that related to C is $\mathbf{v}_C$. Babinet's principle as given by Gangi and Mohanty[4] states that the total fields on the opposite sides of the screens from the source satisfy

$$\mathbf{v}_S+\mathbf{v}_C=\mathbf{v}_0, \tag{12}$$

where $\mathbf{v}_0$ is the field in the absence of any screen. Equation (12) states that the diffraction fields for the complementary screens will be the negative of each other. Moreover, the total fields on the source side must satisfy

$$\mathbf{v}_S+\mathbf{v}_C=2\mathbf{v}_0+\mathbf{v}_R, \tag{13}$$

where $\mathbf{v_R}$ is the reflected (and diffracted) field by a screen composed of S and C if they have different boundary conditions, and it is just the reflected field if they have the same boundary condition.

III. SCREEN MODELING BY DOMAIN DECOMPOSITION

Consider a planar interface in an anisotropic medium, with the symmetry axis perpendicular to the interface plane. The medium may not necessarily be homogeneous. Assume the two-dimensional case, and refer to the upper and lower half-spaces with the labels I and II, respectively, with z increasing toward the upper medium.

The screen model is implemented in numerical modeling by using a domain-decomposition technique. Carcione[6] and Tessmer *et al.*[8] applied the method to model elastic waves across a welded interface between two elastic half-spaces and across an interface separating an acoustic layer from an elastic medium (where v_x need not be continuous). The boundary treatment is based on characteristics representing one-way waves propagating with the phase velocity of the medium. The wave equation is decomposed into outgoing- and incoming-wave modes perpendicular to the interface separating the two half-spaces. The outgoing waves are de-

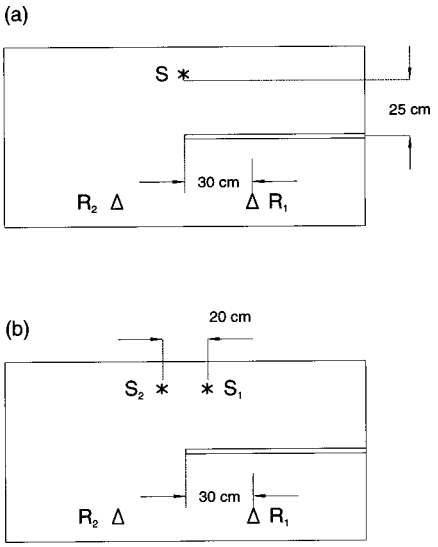

FIG. 1. Source–receiver configurations for the numerical experiments corresponding to the laboratory tests B (a) and A (b) performed by Gangi and Mohanty.[4] In (a), the fields detected by receiver R_1 and R_2 correspond to complementary screens if the medium is isotropic or transversely isotropic with its symmetry axis normal to the screen plane.

termined by the solution inside the corresponding half-space, while the incoming waves are calculated from the boundary conditions.

Most explicit time-integration schemes compute the operation $\mathbf{Mv} \equiv (\mathbf{v})^{\text{old}}$ where

$$\mathbf{M} = \mathbf{A}\frac{\partial}{\partial x} + \mathbf{B}\frac{\partial}{\partial z}. \tag{14}$$

The vector $(\mathbf{v})^{\text{old}}$ is then updated by the boundary treatment to give a new vector $(\mathbf{v})^{\text{new}}$ that takes into account the boundary conditions. The boundary equations are given in the Appendix.

The velocity–stress Eq. (1) is solved by a fourth-order Runge–Kutta time-integration algorithm. The spatial derivatives, that is, the operation with **M** on the field variables, are computed by using the Fourier method in the horizontal direction, and the Chebyshev method in the vertical directions, where nonperiodic boundary conditions are required. After an operation with **M**, the field variables are updated by using the equations given in the Appendix. More details about the numerical technique can be found, for instance, in Carcione.[7,12]

IV. MODEL AND MODELING SETUP

The model simulates the laboratory tests performed by Gangi and Mohanty[4] in a homogeneous and elastic isotropic material (P–S propagation), and in addition, SH propagation through the symmetry plane of a monoclinic medium and qP–qS propagation in a transversely isotropic solid whose symmetry axis is perpendicular to the screen plane. The source–receiver configurations illustrated in Fig. 1(a) and (b) are used to test Babinet's principle. They correspond to configurations B and A in Gangi and Mohanty,[4] respectively.

The calculations use two meshes with $N_x = 375$ and $N_z = 81$ each, and a horizontal grid spacing of 4.7 mm. The maximum vertical grid spacings are 7.1 and 7.35 mm, respectively. The source and receiver positions and the screen tip should be carefully determined, since a small difference can produce a big difference when comparing amplitudes of diffracted arrivals at the receivers. In number of grid points, the screen begins at the (horizontal) grid point 187. This means that the tip is in between points 186 and 187. Thus, taking this fact into account, source S in configuration B is applied at points 186 and 187, and sources S_1 and S_2, corresponding to configuration A, are located at grid points 208 and 165, respectively. Moreover, the positions of receivers R_1 and R_2 are in grid points 208 and 165, respectively. The vertical location of sources and receivers does not have a major influence on the calculations. The source emits a pulse of peak frequency $f_0 = 33$ KHz with a duration of approximately 68 μs. If time t is given in μs, the time history is

$$(1 - 2\alpha t^2)\exp(-\alpha t^2), \quad \alpha = 1/150.$$

A delay of 34.5 μs is applied to the pulse, to make it causal.

In order to better resolve the different events, a denser mesh is used for testing the principle with configuration B. In this case, $N_x = 625$, $N_z = 161$, with a horizontal grid spacing of 2.82 mm, and maximum vertical grid spacings of 3.55 and 3.65 mm, respectively. The source emits a pulse of peak frequency $f_0 = 52$ kHz with a duration of approximately 45 μs. The time history is obtained from the previous expression, with $\alpha = 2/75$. Causality requires a delay of 23.1 μs.

Open-radiation conditions and absorbing strips of width 18 grid points are implemented at the outer horizontal boundaries. At the sides, absorbing strips of the same width are used in order to eliminate wraparound effects caused by the Fourier operator. The solution is propagated to 900 ms with a time step of 0.3 μs and resampled to 1.2 μs.

V. TEST OF THE RECIPROCITY PRINCIPLE

A first numerical experiment tests the modeling algorithm by verifying the reciprocity principle.[13,14] Seismic reciprocity implies that sources and receivers can be interchanged under certain conditions. This relationship holds for an elastic medium with arbitrary boundary conditions, inhomogeneity, and anisotropy. In our experiments, the homogeneity is broken by the presence of the screen.

The test uses configuration A and compares the horizontal particle velocity v_x at R_1 caused by a vertical force at S_1, with the vertical particle velocity v_z at S_1 due to a horizontal source at R_1. The comparison is shown in Fig. 2, where the dotted line corresponds to the horizontal source. The matching is excellent, and provides a partial verification of the modeling algorithm.

VI. TEST OF BABINET'S PRINCIPLE

The following numerical experiments test the validity of Babinet's principle for complementary screens of the same type, i.e., both stress-free (weak) or both rigid, and for screens having different properties; that is, if the original screen is rigid (stress-free), the complementary screen may be stress-free (rigid). The qP–qS anisotropic case considers a crack embedded in a transversely isotropic medium.

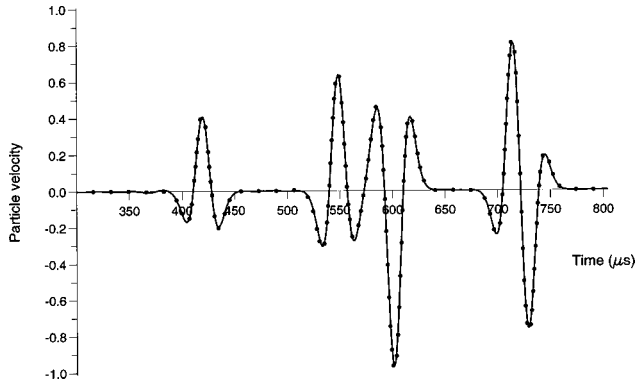

FIG. 2. Verification of the reciprocity principle using configuration A [Fig. 1(b)]. The test compares the horizontal-particle velocity v_x at R_1 caused by a vertical force at S_1 (continuous line) with the vertical-particle velocity v_z at S_1 due to a horizontal source at R_1 (dots).

A. The anisotropic SH case

We consider configuration B and a monoclinic medium with $C_{44}=\rho V_{44}^2$, $C_{66}=\rho V_{66}^2$, and $C_{46}=0.5\rho V_{44}^2$, where $V_{66}=1300$ m/s, $V_{44}=970$ m/s, and $\rho=1$ g/cm^3 ($\theta\approx 45$ deg). Since the problem is not symmetric (the elliptical-wave surface is tilted with respect to the z-axis), the measurements at R_2 (R_1) in Fig. 1(a) do not provide the values corresponding to the complementary screen of the same type, when testing the principle at R_1 (R_2). Instead, the simulation with a complementary screen from grid point 1 to grid point 186 is required. The experiment consists of five simulations, two with rigid boundary conditions, with the screen at the left side and the right side of the plane, respectively, two with stress-free boundary conditions, and one unscreened.

Figure 3 compares scattered pulses (diffracted at the tip) at R_1 (580-μs onset) and R_2 (730-μs onset) for complementary screens of different type, i.e., stress-free and rigid. Figure 3(a) [(b)] corresponds to the weak screen at the right (left) side and the rigid screen at the left (right) side. The scattered field at receivers R_1 and R_2 for the rigid–left (weak–left) and weak–right (rigid–right) cases are obtained by subtracting the total field to the unscreened field (no screen present). As can be seen, there is an excellent match when the original screen is rigid (weak) and the complementary screen is weak (rigid), demonstrating that, in this case, Babinet's principle holds for screens of different type. This result is in agreement with the proof by Jones[3] in the purely acoustic case (pressure waves).

B. The elastic case

1. Isotropic media

The set of numerical experiments performed by Gangi and Mohanty[4] uses polystyrene (80 cm wide by 160 cm long) whose compressional and shear velocities are $V_P=Z_P/\rho=1750$ m/s and $V_S=Z_S/\rho=970$ m/s, respectively, with a density $\rho=1$ g/cm^3. Figure 4(a) represents the particle velocity v_z recorded at receivers R_1 for a weak screen (broken line) and R_2 for a rigid screen (continuous line), corresponding to configuration B. P and S are the direct arrivals and *d*, *r*, and *c* denote diffracted, refracted, and critical, respectively. For instance, PdPrSc is the compressional wave

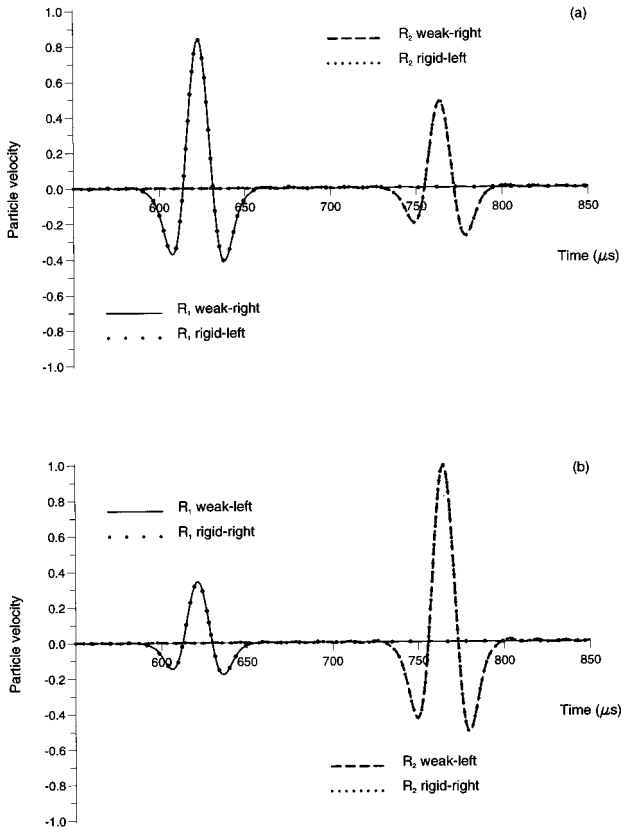

FIG. 3. Test of Babinet's principle for SH waves propagating in a monoclinic medium, corresponding to configuration B. The figure shows the scattered pulses at R_1 (580-μs onset) and R_2 (730-μs onset) for complementary screens of different type, i.e., stress-free and rigid. Figure 3(a) [(b)] corresponds to the weak screen at the right (left) side and the rigid screen at the left (right) side. The scattered field at receivers R_1 and R_2 for the rigid–left (weak–left) and weak–right (rigid–right) cases are obtained by subtracting the total field from the field obtained in the unscreened case (no screen present).

refracted along the screen plane and then incident at the receiver at the critical angle (i.e., a conical or lateral wave). Note that receiver R_1 records diffractions only. Figure 4(b) compares the unscreened field at R_2 (continuous line) to the field recorded at R_2 (rigid screen; direct arrivals plus diffractions) minus the field recorded at R_1 (weak screen; diffractions plus lateral waves). It is clear that Babinet's principle is not satisfied by the lateral wave PdPrSc, since this event is only recorded at R_1. This is evident in Fig. 5(a), which compares the scattered pulses at R_1 (continuous line) and R_2 (dotted line). As can be seen, there is no doubt that the PdP wave and the SdS wave (not visible in Fig. 4) satisfy the principle (for complementary screens of different type). Figure 5(b) represents the scattered pulse for weak complementary screens with the continuous line corresponding to R_1 and the dotted line to R_2. In this case, the principle is not satisfied.

Numerical experiments for configuration A are represented in Fig. 6, where (a) compares scattered events at R_1 (continuous line) and R_2 (dotted line) for complementary screens of the different type (weak screen and source S_1, and rigid screen and source S_2, respectively), and (b) compares scattered events for screens of equal type (weak screens for sources S_1 and S_2). The pulses correspond to the v_x compo-

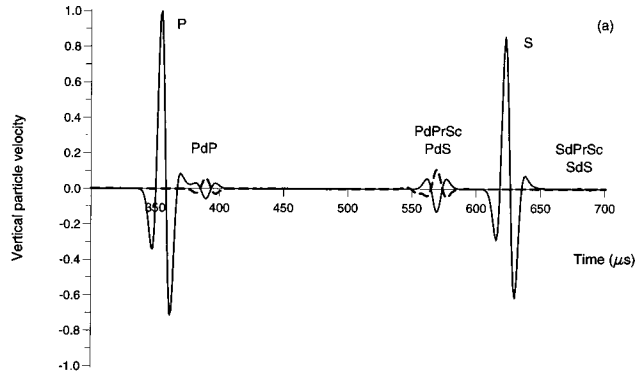

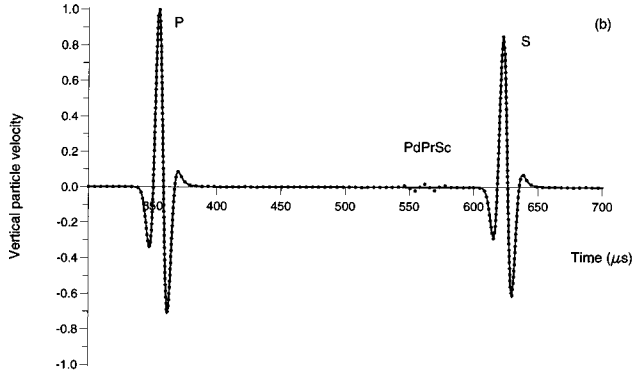

FIG. 4. Test of Babinet's principle for P–S waves propagating in an isotropic medium, where (a) shows the particle velocity v_z recorded at receivers R_1 for a weak screen (broken line) and R_2 for a rigid screen (continuous line), corresponding to configuration B. P and S are the direct arrivals and *d*, *r*, and *c* denote diffracted, refracted, and critical, respectively. (b) Compares the unscreened field at R_2 (continuous line) to the field recorded at R_2 (rigid screen; direct arrivals plus diffractions) minus the field recorded at R_1 (weak screen; diffractions plus lateral waves).

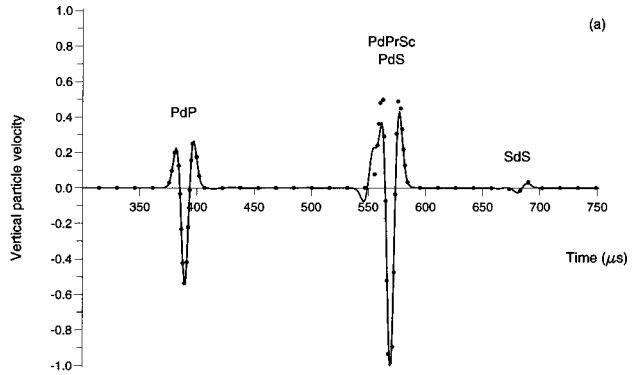

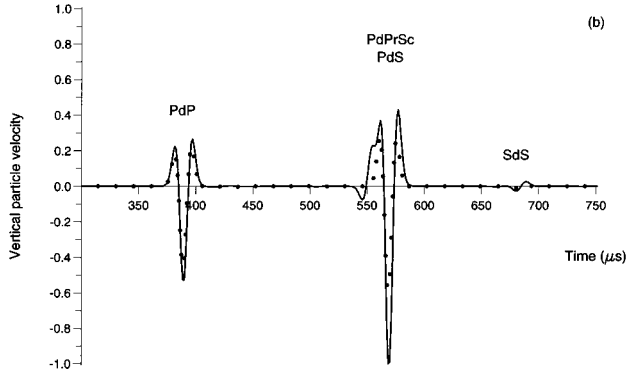

FIG. 5. Test of Babinet's principle for P–S waves propagating in an isotropic medium. (a) Compares the scattered pulses at R_1 (weak screen, continuous line) and R_2 (rigid screen, dotted line), while (b) represents the scattered pulse for weak complementary screens, with the continuous line corresponding to R_1 and the dotted line to R_2.

nent of the wave field. As before, the PdP wave satisfies the principle for the mixed case, as well as the SdP diffraction, not observed in configuration B. The mismatch is due to the presence of lateral waves. In particular, the SdPrSc event is much stronger than the SdS at receiver R_1. This can be appreciated in the snapshot displayed in Fig. 7, which shows the v_x component at 510 μs for a weak screen and source S_2. The PdPrSc and SdPrSc are the planar wavefronts below the screen, which are tangent to the PdS and SdS cylindrical wavefronts, respectively. The two larger cylindrical wavefronts correspond to the direct P and S waves, respectively.

2. Anisotropic media

A transversely isotropic medium is defined by the elastic constants $c_{11}=1.4\rho V_P^2$, $c_{33}=\rho V_P^2$, $c_{13}=0.08c_{33}$, and $c_{55}=\rho V_S^2$, with V_P and V_S as in the isotropic case. For illustration, Fig. 8 shows a polar representation of the energy (group) velocity corresponding to the qP (quasicompressional) and qS (quasishear) waves, where the vertical axis is the symmetry axis perpendicular to the plane of isotropy (by symmetry considerations, only one-quarter of the plane is displayed). Babinet's principle is tested in the presence of a crack, located between points 150 and 223. A snapshot of the v_z component at 510 μs can be seen in Fig. 9, with the crack plane satisfying stress-free boundary conditions. Rayleigh waves traveling along this plane can be appreciated in the snapshot. Note the strong cuspidal triangle of the shear wave that triplicates in the direction of the receiver (see also Fig. 8). Figure 10(a) represents the particle velocity v_z for the crack (broken line) and the hole (continuous line), i.e., the ''complementary crack,'' and Fig. 10(b) compares the unscreened field (continuous line) to the field obtained by substracting the two pulses represented in Fig. 10(a) (dotted line). Due to the particular source–receiver configuration, the diffractions are very close to the respective direct arrivals which generate them. The PdS diffraction can be clearly seen in Fig. 9 between the P and S waves. The stronger peak is the cusp of the shear wave, which due to triplication is followed by a weaker event arriving at approximately 550 μs. Figure 11 represents the scattered pulses, where the continuous line corresponds to the crack and the dotted line to the hole. The good matching between traces implies that Babinet's principle is satisfied also in the case of shear-wave triplication. The small differences may be due to the presence of weak lateral waves generated at the left tip of the crack.

VII. CONCLUSIONS

We have investigated Babinet's principle for elastic waves by using a numerical simulation technique. The method for solving wave propagation uses a domain-decomposition technique that assigns a different mesh to

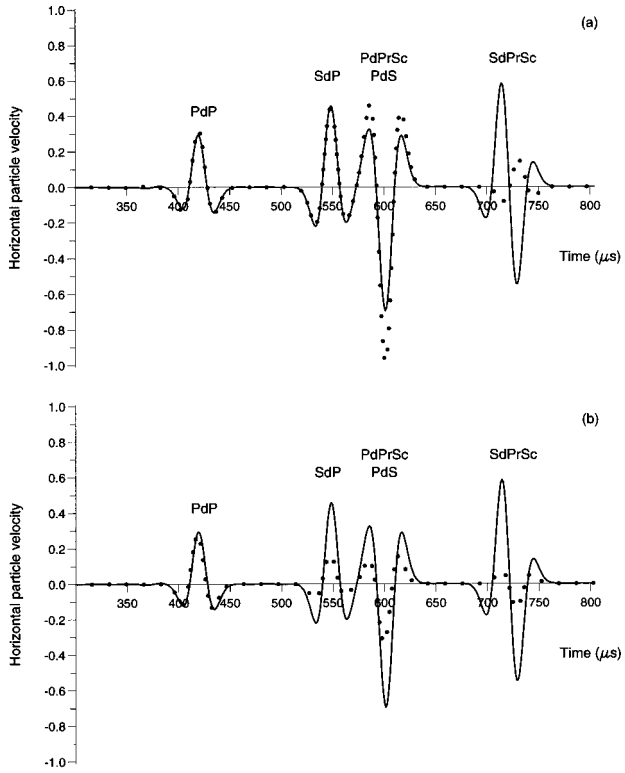

FIG. 6. Numerical experiments displaying the v_z component for configuration A, where (a) compares scattered events at R_1 (continuous line) and R_2 (dotted line) for complementary screens of different type (weak screen and source S_1, and rigid screen and source S_2, respectively), and (b) compares scattered events for screens of equal type (weak screens for sources S_1 and S_2).

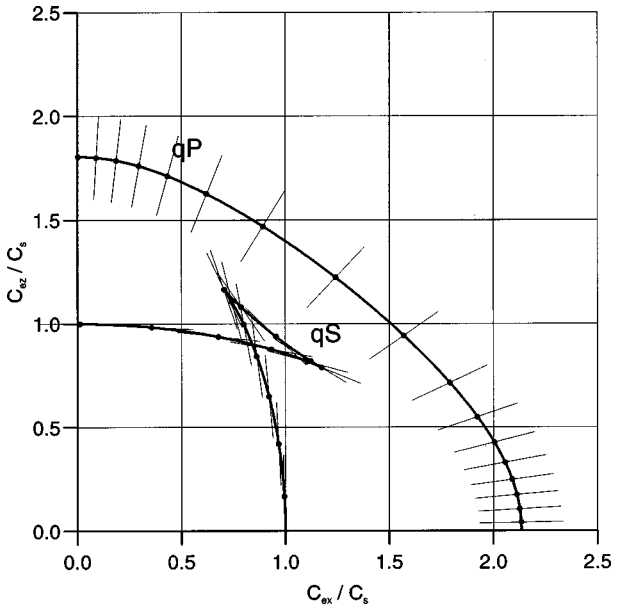

FIG. 8. Polar representation of the energy (group) velocity corresponding to the qP (quasicompressional) and qS (quasishear) waves, where the vertical axis is the symmetry axis perpendicular to the plane of isotropy (from symmetry considerations, only one-quarter of the plane is displayed).

each side of the screen plane. The use of the Chebyshev differential operator, to compute the spatial derivatives normal to the interface, allows the imposition of general boundary conditions. A first numerical experimental provides a partial verification of the modeling algorithm by testing the reciprocity principles in the presence of a stress-free screen.

In electromagnetics, Babinet's principle for infinitely thin perfectly conducting complementary screens implies that the sum, beyond the screen plane, of the electric and the magnetic fields (adjusting physical dimensions) equals the incident (unscreened) electric field. In elastodynamics, the principle holds for the same field (particle velocity or stress), but for complementary screens satisfying different types of boundary conditions, i.e., if the original screen is weak (rigid), the complementary screen must be rigid (weak).

We have shown that Babinet's principle holds for screens embedded in anisotropic media, both for SH and qP–qS waves. Five simulations are required to test the principle for SH waves propagating in the plane of mirror symmetry of a monoclinic medium (the elliptical-wave surface is tilted with respect to the screen plane). The simulations indicate that Babinet's principle is satisfied also in the case of

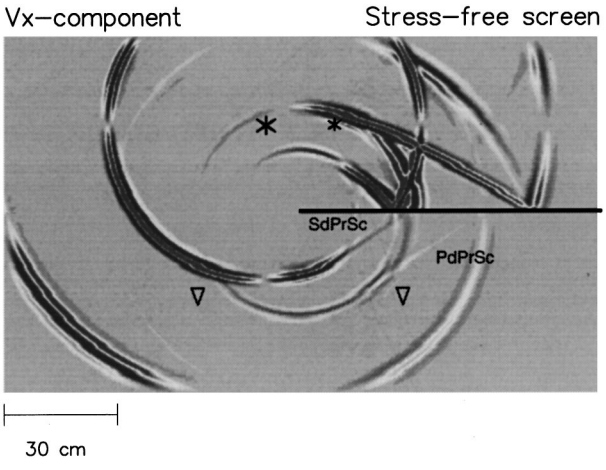

FIG. 7. Snapshot of the v_x component at 510 μs for a weak screen and source S_2. The PdPrSc and SdPrSc are conical waves, which are tangent to the PdS and SdS cylindrical wavefronts, respectively. The two larger cylindrical wavefronts correspond to the direct P and S waves, respectively.

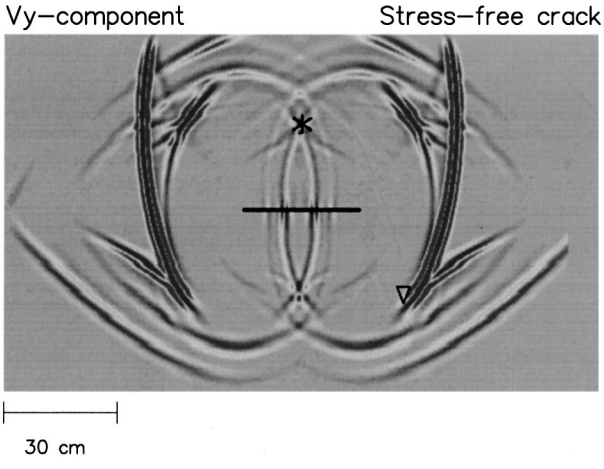

FIG. 9. Snapshot of the v_z component at 510 μs in a transversely isotropic medium, with the crack plane satisfying stress-free boundary conditions. Rayleigh waves traveling along this plane can be appreciated. The strong cuspidal triangle of the shear wave triplicates along the direction of the receiver.

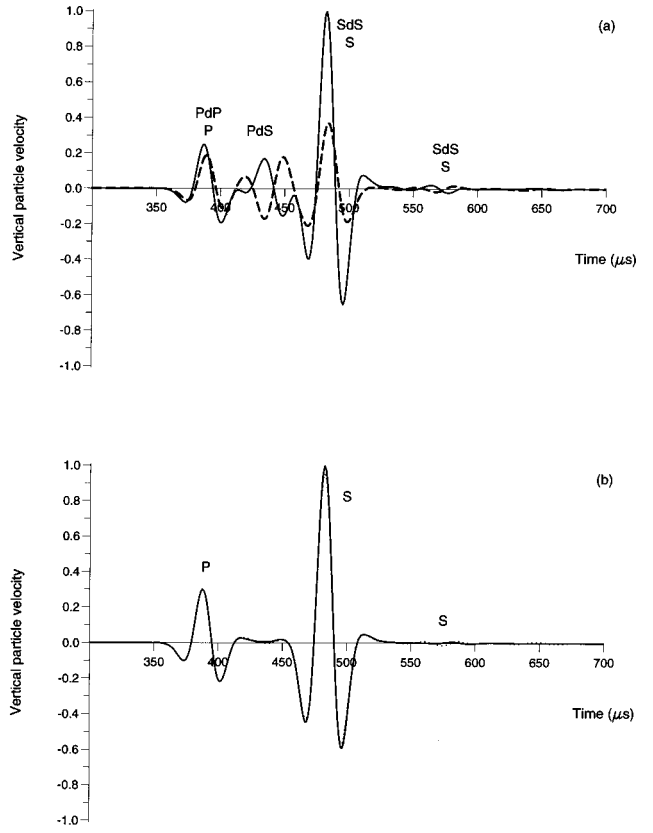

FIG. 10. Test of Babinet's principle for qP–qS waves propagating through a crack imbedded in a transversely isotropic medium. In (a), the particle velocity v_z corresponding to the crack (broken line) and the hole (continuous line) are represented. (b) Compares the unscreened field (continuous line) to the field obtained by subtracting the two pulses represented in (a) (dotted line).

shear-wave triplications (qS waves). Moreover, the experiments show that Babinet's principle holds for the near and far fields, and for an arbitrary pulse waveform and frequency spectrum. However, as expected, lateral and interface (e.g., Rayleigh) waves do not satisfy the principle.

Further research will involve the analysis of Babinet's principle for an inhomogeneous and/or viscoelastic background medium, screens separating a fluid and solid, and nonplanar screens. Moreover, a mathematical demonstration is required to prove that interface and lateral waves do not satisfy the principle.

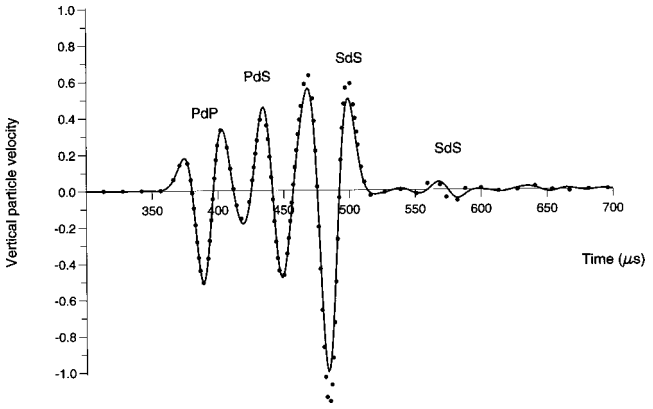

FIG. 11. Scattered pulses for the transversely isotropic case. The continuous line corresponds to the crack and the dotted line to the hole. The good matching between traces implies that Babinet's principle is also satisfied in the case of shear-wave triplication.

APPENDIX: BOUNDARY EQUATIONS FOR ANISOTROPIC MEDIA

The following equations model the different boundary conditions between two half-spaces. In general, they were published for an isotropic medium. This Appendix extends the theory to a monoclinic medium for pure shear waves and to a transversely isotropic medium with the symmetry axis perpendicular to the screen plane for qP and qS waves.

1. The *SH* case

The domain-decomposition equations for SH waves resemble those of the acoustic case given in Carcione.[6] A similar analysis yields for a *welded* interface:

$$(v)_{\mathrm{I}}^{\mathrm{new}}=\tfrac{1}{2}\{(v)_{\mathrm{II}}^{\mathrm{old}}+(v)_{\mathrm{I}}^{\mathrm{old}}+Z_{44}^{-1}[(\sigma_{zy})_{\mathrm{II}}^{\mathrm{old}}+(\sigma_{zy})_{\mathrm{I}}^{\mathrm{old}}]\}, \tag{A1}$$

$$(\sigma_{zy})_{\mathrm{I}}^{\mathrm{new}}=\tfrac{1}{2}\{Z_{44}[(v)_{\mathrm{II}}^{\mathrm{old}}+(v)_{\mathrm{I}}^{\mathrm{old}}]+(\sigma_{zy})_{\mathrm{I}}^{\mathrm{old}}+(\sigma_{zy})_{\mathrm{II}}^{\mathrm{old}}\}, \tag{A2}$$

$$(\sigma_{xy})_{\mathrm{I(II)}}^{\mathrm{new}}=(\sigma_{xy})_{\mathrm{I(II)}}^{\mathrm{old}}-\frac{C_{46}}{C_{44}}[(\sigma_{zy})_{\mathrm{I(II)}}^{\mathrm{old}}-(\sigma_{zy})_{\mathrm{I(II)}}^{\mathrm{new}}], \tag{A3}$$

$$(v)_{\mathrm{II}}^{\mathrm{new}}=(v)_{\mathrm{I}}^{\mathrm{new}},\quad (\sigma_{zy})_{\mathrm{II}}^{\mathrm{new}}=(\sigma_{zy})_{\mathrm{I}}^{\mathrm{new}}, \tag{A4}$$

where

$$Z_{44}=\sqrt{C_{44}\rho}. \tag{A5}$$

The relations for the *stress-free* case are

$$(v)^{\mathrm{new}}=(v)^{\mathrm{old}}\mp Z_{44}^{-1}(\sigma_{zy})^{\mathrm{old}}, \tag{A6}$$

$$(\sigma_{zy})^{\mathrm{new}}=0, \tag{A7}$$

$$(\sigma_{xy})^{\mathrm{new}}=(\sigma_{xy})^{\mathrm{old}}-\frac{C_{46}}{C_{44}}(\sigma_{zy})^{\mathrm{old}}, \tag{A8}$$

where the $-$ sign corresponds to half-space I and the $+$ sign to half-space II.

The updated variables for the *rigid* case are

$$(v)^{\mathrm{new}}=0, \tag{A9}$$

$$(\sigma_{zy})^{\mathrm{new}}=(\sigma_{zy})^{\mathrm{old}}\mp Z_{44}(v)^{\mathrm{old}}, \tag{A10}$$

including Eq. (A8) and the same sign convention as before.

2. The qP–qS case

The characteristic waves for anisotropic media were obtained by Tessmer[15] and Carcione.[6,7] Carcione[6] obtained the boundary equations in the case of two *welded* isotropic media. Extension to the transversely isotropic case with the symmetry axis perpendicular to the interface yields

$$(v_x)_{\mathrm{I}}^{\mathrm{new}}=\frac{1}{2Z_{\mathrm{S}}}\{Z_{\mathrm{S}}(v_x)_{\mathrm{I}}^{\mathrm{old}}+Z_{\mathrm{S}}(v_x)_{\mathrm{II}}^{\mathrm{old}}-(\sigma_{xz})_{\mathrm{I}}^{\mathrm{old}}+(\sigma_{xz})_{\mathrm{II}}^{\mathrm{old}}\}, \tag{A11}$$

$$(v_z)_{\rm I}^{\rm new}=\frac{1}{2Z_{\rm P}}\{Z_{\rm P}(v_z)_{\rm I}^{\rm old}+Z_{\rm P}(v_z)_{\rm II}^{\rm old}-(\sigma_{zz})_{\rm I}^{\rm old}+(\sigma_{zz})_{\rm II}^{\rm old}\}, \tag{A12}$$

$$(\sigma_{xx})_{\rm I}^{\rm new}=(\sigma_{xx})_{\rm I}^{\rm old}+\frac{c_{13}}{c_{33}}[(\sigma_{zz})_{\rm I}^{\rm new}-(\sigma_{zz})_{\rm I}^{\rm old}], \tag{A13}$$

$$(\sigma_{zz})_{\rm I}^{\rm new}=\tfrac{1}{2}\{Z_{\rm P}[(v_z)_{\rm II}^{\rm old}-(v_z)_{\rm I}^{\rm old}]+(\sigma_{zz})_{\rm I}^{\rm old}+(\sigma_{zz})_{\rm II}^{\rm old}\}, \tag{A14}$$

$$(\sigma_{xz})_{\rm I}^{\rm new}=\tfrac{1}{2}\{Z_{\rm S}[(v_x)_{\rm II}^{\rm old}-(v_x)_{\rm I}^{\rm old}]+(\sigma_{xz})_{\rm I}^{\rm old}+(\sigma_{xz})_{\rm II}^{\rm old}\}, \tag{A15}$$

$$(v_x)_{\rm II}^{\rm new}=(v_x)_{\rm I}^{\rm new},\quad (v_z)_{\rm II}^{\rm new}=(v_z)_{\rm I}^{\rm new}, \tag{A16}$$

$$(\sigma_{xx})_{\rm II}^{\rm new}=(\sigma_{xx})_{\rm II}^{\rm old}+\frac{c_{13}}{c_{33}}[(\sigma_{zz})_{\rm II}^{\rm new}-(\sigma_{zz})_{\rm II}^{\rm old}], \tag{A17}$$

$$(\sigma_{zz})_{\rm II}^{\rm new}=(\sigma_{zz})_{\rm I}^{\rm new},\quad (\sigma_{xz})_{\rm II}^{\rm new}=(\sigma_{xz})_{\rm I}^{\rm new}, \tag{A18}$$

where

$$Z_{\rm P}=\sqrt{c_{33}\rho}\quad\text{and}\quad Z_{\rm S}=\sqrt{c_{55}\rho}, \tag{A19}$$

are the compressional and shear impedances along the z-axis, respectively. In the isotropic case, $c_{11}=c_{33}$ and $c_{13}=Z_{\rm P}^2-2Z_{\rm S}^2$.

The relations for the *stress-free* case are[15,7]

$$(v_x)^{\rm new}=(v_x)^{\rm old}\mp Z_{\rm S}^{-1}(\sigma_{xz})^{\rm old}, \tag{A20}$$

$$(v_z)^{\rm new}=(v_z)^{\rm old}\mp Z_{\rm P}^{-1}(\sigma_{zz})^{\rm old}, \tag{A21}$$

$$(\sigma_{xx})^{\rm new}=(\sigma_{xx})^{\rm old}+\frac{c_{13}}{c_{33}}[(\sigma_{zz})^{\rm new}-(\sigma_{zz})^{\rm old}], \tag{A22}$$

$$(\sigma_{xz})^{\rm new}=0, \tag{A23}$$

$$(\sigma_{zz})^{\rm new}=0, \tag{A24}$$

where the $-$ sign corresponds to half-space I and the $+$ sign to half-space II.

The updated variables for the *rigid* case are[7]

$$(v_x)^{\rm new}=0, \tag{A25}$$

$$(v_z)^{\rm new}=0, \tag{A26}$$

$$(\sigma_{xx})^{\rm new}=(\sigma_{xx})^{\rm old}+\frac{c_{13}}{c_{33}}[(\sigma_{zz})^{\rm new}-(\sigma_{zz})^{\rm old}], \tag{A27}$$

$$(\sigma_{xz})^{\rm new}=(\sigma_{xz})^{\rm old}\mp Z_{\rm S}(v_x)^{\rm old}, \tag{A28}$$

$$(\sigma_{zz})^{\rm new}=(\sigma_{zz})^{\rm old}\mp Z_{\rm P}(v_z)^{\rm old}, \tag{A29}$$

with the same sign convention as before.

[1] P. Epstein, Enzyl. d. Math. Wissensch., Bd. 5, Art. 24, SS. 510–511, Leipzig (1915).
[2] L. G. H. Huxley, *A Survey of the Principles and Practice of Wave Guides* (MacMillan, New York, 1947).
[3] D. S. Jones, *Acoustic and Electromagnetic Waves* (Oxford Science, New York, 1986).
[4] A. F. Gangi and B. B. Mohanty, ''Babinet's principle for elastic waves,'' J. Acoust. Soc. Am. **53**, 525–534 (1973).
[5] A. F. Gangi, ''A derivation of the seismic representation theorem using seismic reciprocity,'' J. Geophys. Res. **75**(11), 2088–2095 (1970).
[6] J. M. Carcione, ''Domain decomposition for wave propagation problems,'' J. Sci. Comput. **6**, 453–472 (1991).
[7] J. M. Carcione, ''Time-dependent boundary conditions for the 2-D linear anisotropic–viscoelastic wave equation,'' Numer. Meth. Part. Diff. Eqs. **10**, 771–791 (1994).
[8] E. Tessmer, D. Kessler, D. Kosloff, and A. Behle, ''Multi-domain Chebyshev–Fourier method for the solution of the equations of motion of dynamic elasticity,'' J. Comput. Phys. **100**, 355–363 (1992).
[9] R. D. Borcherdt, ''Reflection and refraction of type-II *S* waves in elastic and anelastic media,'' Bull. Seismol. Soc. Am. **67**, 43–67 (1977).
[10] J. M. Carcione, ''Wavefronts in dissipative anisotropic media,'' Geophysics **59**, 644–657 (1994).
[11] K. Helbig, *Foundations of Anisotropy for Exploration Seismics* (Pergamon, New York, 1994).
[12] J. M. Carcione, ''A 2-D Chebyshev differential operator for the elastic wave equation,'' Comput. Methods Appl. Mech. Eng. **130**, 33–45 (1996).
[13] D. Graffi, ''Sui teoremi di reciprocità nei fenomeni indipendenti dal tempo,'' Ann. Math. **18**, 173–200 (1939).
[14] L. Knopoff and A. F. Gangi, ''Seismic reciprocity,'' Geophysics **24**, 681–691 (1959).
[15] E. Tessmer, ''Seismische Modellierung unter Berücksichtigung der freien Oberfläche mithilfe spektralen Tschebyscheff-Methode,'' Ph.D. thesis, Hamburg University, 1990.